SURROGATE-DRIVEN MOTION MODEL FOR MOTION COMPENSATED CONE-BEAM CT RECONSTRUCTION USING UNSORTED PROJECTION DATA

Yuliang Huang[1,2] *Kris Thielemans*[1,3] *Jamie R. McClelland*[1,2]

[1] Centre for Medical Image Computing, University College London, London, UK
[2] Wellcome and EPSRC Centre for Surgical and Interventional Sciences, University College London, London, UK
[3] Institute of Nuclear Medicine, University College London, London, UK

2023 IEEE 20th International Symposium on Biomedical Imaging (ISBI) | 978-1-6654-7358-3/23/$31.00 ©2023 IEEE | DOI: 10.1109/ISBI53787.2023.10230761

ABSTRACT

Cone-beam CT (CBCT) is widely used in image guided radiotherapy, but motion due to breathing can blur the image. Similar to 4DCT, 4D CBCT can reduce motion blur but 4D CBCT acquisitions take 2~4 times longer than 3D CBCT and often suffer from phase sorting artefact. This study aims to obtain motion models and motion-free images simultaneously from unsorted 3D CBCT projection data, using a general motion modelling framework previously proposed by our group, which was for the first time successfully applied to real CBCT data equivalent to a one-minute acquisition. The performance of our method was comprehensively evaluated through digital phantom simulation and also validated on real patient data. This study demonstrated the feasibility of our proposed framework for simultaneous motion model fitting and motion compensated reconstruction using unsorted 3D CBCT projection data.

Index Terms— Motion compensation, respiration surrogate, motion model, unified framework, CBCT

1. INTRODUCTION

Cone-beam CT has been widely used in image-guided radiotherapy to ensure radiation dose is delivered to the tumor. However, any motion, such as respiratory motion, could lead to artifacts and affect the image quality of CBCT images [1]. To address this problem, more CBCT projections can be acquired over a longer acquisition time and then sorted into multiple respiratory phases (normally 6 10 phases) to obtain 4DCBCT [2], i.e., a series of CBCT images reconstructed out of projection subsets that belong to each respiratory phase. Nevertheless, 4DCBCT suffers from severe streak artifact due to the uneven angular distribution of projections within each phase [3], and breath-to-breath variability and sorting errors can lead to residual blurring. Moreover, the longer acquisition time of 4DCBCT was not preferable in clinical practice and associated with more imaging dose to patients [4].

In comparison to 4DCBCT, motion compensated approaches use all the projection data instead of a subset to reconstruct a single reference state image $\mathbf{I_0}$ by considering the motion at every timepoint with respect to the reference state image [5, 6]. The image at a specific time point $\mathbf{I_t}$ can be obtained by warping $\mathbf{I_0}$ according to the motion at that timepoint. Since all the projections are used for reconstruction, acquisition time can be shortened and streak artifacts reduced, but the difficulty of this approach lies in estimating the motion at every timepoint.

Some methods estimated the motion from the planning 4DCT scan [7], but changes of the motion pattern and/or anatomy between the 4DCT and CBCT scan could limit the accuracy of such approaches. Projection-based methods may be more suitable for estimating motion during CBCT acquisition since the projections are the direct measured data. Under this approach, the optimal deformation vector field (DVF) is solved by maximizing the similarity between a projection of the warped reference image and the measured projection. Wang and Gu proposed the SMEIR algorithm [8] which combined projection-based motion estimation with motion compensated reconstruction to iteratively update the DVF and reference image. The method still required phase-binning of the projection and thus assumed reproducible breathing, which is not always a valid assumption for lung cancer patients [9]. Instead, Jailin et al estimated the DVF corresponding to every single projection without requiring phase sorting [10], giving very promising results but requiring long computation time.

Surrogate driven motion models [11] are another method that can provide DVFs at each frame in a more intuitive way than the one described in [10]. In this approach, the motion is parameterized by one or more respiratory surrogate signals which can be acquired from external devices, such as marker(s) on the skin surface [12], or derived directly from the projection data [13].

However, the traditional way of fitting a surrogate driven motion model requires first estimating the 3D motion at each timepoint e.g. using image registration [11], which made it less applicable to projection data. In recent years our group has been developing a general motion model framework that unified motion model fitting with image registration and mo-

tion compensated reconstruction, enabling the method to be applied on unreconstructed 'raw' data such as CBCT projections [14].

In this study, the general framework was applied to CBCT projection data and evaluated systematically by numerical simulation. More importantly, the feasibility of this method is demonstrated on clinical data for the first time. Using our method, dynamic images that showed the respiration motion of lung cancer patients can be generated from nothing more than unsorted CBCT projection equal to a 1-minute acquisition.

2. METHOD AND MATERIAL

2.1. General Motion Model Framework

Given a set of 2D CBCT projection images ($\mathbf{P_t}$), the goal of this study is to obtain a motion-free CBCT image ($\mathbf{I_0}$) and a time series of DVFs $\mathbf{D_t}$ that can warp the reference state image $\mathbf{I_0}$ to the CBCT image ($\mathbf{I_t}$) at the moment when each projection was acquired, as shown by equation (1)

$$\mathbf{I_t} = T(\mathbf{I_0}, \mathbf{D_t}) \tag{1}$$

where T is a function that resamples $\mathbf{I_0}$ according to the spatial transform determined by $\mathbf{D_t}$ at time-point t.

This study used free-form deformations, in which the deformation is obtained from B-spline transformation:

$$\mathbf{D_t} = \phi(\mathbf{M_t}) \tag{2}$$

where $\mathbf{M_t}$ is the control point parameters of B-spline transformation. The surrogate-driven respiration correspondence model can then be represented as follows:

$$\mathbf{M_t} = \mathbf{S_t} \cdot \mathbf{C} = \Sigma_i^r S_{it} \cdot \mathbf{C_i} \tag{3}$$

in which r is the number of surrogate signals, S_{it} is the i^{th} surrogate signal at time-point t and $\mathbf{C_i}$ is the i^{th} component of correspondence model parameters.

The motion model parameters $\mathbf{C}$ can be determined by minimizing the loss function below:

$$f = -\Sigma_t L(\mathbf{P_t}, \mathbf{P'_t}) \tag{4}$$

$$\mathbf{P'_t} = \mathbf{A_t} \cdot \mathbf{I_t} \tag{5}$$

where L refers to localized normalized cross correlation, $\mathbf{P'_t}$ and $\mathbf{P_t}$ are the estimated and measured projection images at time t respectively, and $\mathbf{A_t}$ is the acquisition matrix for CBCT forward projection.

Combining equations (1)-(5), the gradient of the loss function with respect to the motion model parameters could be calculated as follows:

$$\begin{aligned}\frac{\partial f}{\partial \mathbf{C_i}} &= \Sigma_t \frac{\partial \mathbf{M_t}}{\partial \mathbf{C_i}} \cdot \frac{\partial \mathbf{D_t}}{\partial \mathbf{M_t}} \cdot \frac{\partial \mathbf{I_t}}{\partial \mathbf{D_t}} \cdot \frac{\partial \mathbf{P'_t}}{\partial \mathbf{I_t}} \cdot \frac{\partial f}{\partial \mathbf{P'_t}} \\ &= -\Sigma_t S_{it} \cdot \frac{\partial \phi(\mathbf{M_t})}{\partial \mathbf{M_t}} \cdot \frac{\partial T(\mathbf{I_0}, \mathbf{D_t})}{\partial \mathbf{D_t}} \cdot \mathbf{A_t}^* \cdot \frac{\partial L(\mathbf{P_t}, \mathbf{P'_t})}{\partial \mathbf{P'_t}}\end{aligned} \tag{6}$$

where $i = 1, \ldots, r$, and $\mathbf{A_t}^*$ is the adjoint matrix of $\mathbf{A_t}$. In each iteration, the motion model parameters are updated with the gradient above and the step length determined by line search method.

Initially, a standard FDK [15] reconstruction is performed for $\mathbf{I_0}$, and the model parameters $\mathbf{C}$ are updated for a fixed number of iterations, or until there is no improvement in the loss function. The motion model is then used to perform a motion compensated reconstruction of $\mathbf{I_0}$ [5, 6]. The method then proceeds to iteratively update $\mathbf{C}$ and $\mathbf{I_0}$ until there is no further improvement or the total number of iterations are reached. A multi-resolution approach is used, with $\mathbf{P_t}$, $\mathbf{C}$, and $\mathbf{I_0}$ being resampled at each resolution level.

The hyperparameters of this study can be listed as below: number of resolution levels is 3, control point grid spacing is 8 pixels, maximum number of motion compensated reconstruction per level is 6, maximum iteration number of model fitting is 100. To save the runtime, this study just used the first 2 resolution levels for model fitting and only used evenly-spaced stochastic subset (one-tenth of) of time-points per iteration. Compared with the 30 hours runtime in previous study [10], the runtime for our method ranged from 1 to 5 hours, which was one of the major advantages of our method.

2.2. Digital Phantom Simulation

The 4DXCAT software [16, 17] was used to generate a ground truth reference state image and sequence of DVFs from breathing traces that represent the diaphragm and chest surface motion. This study used two sets of real breathing traces, as shown in Figure 1, which were measured from cine sagittal MR slices. The first set of breathing traces showed regular respiration and the other one exhibited a more irregular pattern including hysteresis and inter-cycle variation. For both simulations, the reference state image was warped by the DVF sequence and projection images were generated using the geometry of a real CBCT scan and OpenRTK [18]. The breathing traces were normalized and then used as surrogate signals for motion model fitting.

Our method was tested on these two sets of simulation data using the following metrics:

- DSC: average Dice Similarity Coefficient between estimated and ground-truth tumour masks.
- $\mathrm{E_{center}}$: average Euclidean distance between estimated and ground-truth tumour centroid positions.
- $\mathrm{E_{DVF}}$: DVF error, the average L2-norm of difference between ground-truth and estimated DVF within the body mask.
- NRMSE: root-mean-square error between the reconstructed image and the reconstruction using round-truth DVFs, normalized to the maximum pixel value.

Results of our method were also compared with uncorrected results. The term "uncorrected" means not compensating for motion, or equally speaking, the DVFs at all time-

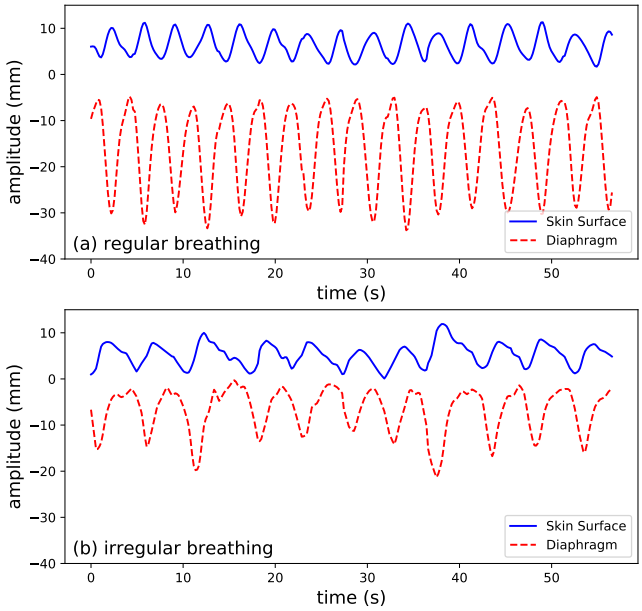

Fig. 1. Two sets of breathing traces for 4DXCAT simulation.

points are zero and the tumour masks at every time-point are the same as the tumour mask on reference state image. The uncorrected CBCT reconstruction refers to standard FDK reconstruction [15] that does not compensate for motion.

2.3. Clinical Dataset

Our method was also validated on real patient data from the public SPARE Challenge dataset [19]. Two patients were selected from the dataset that did not exhibit severe truncation issues in CBCT projections. The CBCT images were acquired over a full rotation on Varian Trilogy with Source-to-Image Distance (SID) of 1000 mm and Source-to-Detector Distance (SDD) of 1500 mm and the detector was offset to enlarge the field-of-view. Dimension and pixel size of the projection images were 1024x768 and 0.388 mm respectively. 680 projections were used, equivalent to a one-minute scan.

As external breathing traces are not available for the SPARE Challenge datasets, this study used the Intensity Analysis (IA) method [13] to extract a respiratory signal directly from the projection images. This signal and its temporal gradient were normalized and then used as the surrogate signal for the two patient datasets. Since no ground-truth was known for clinical data, visual comparison was used to evaluate the results.

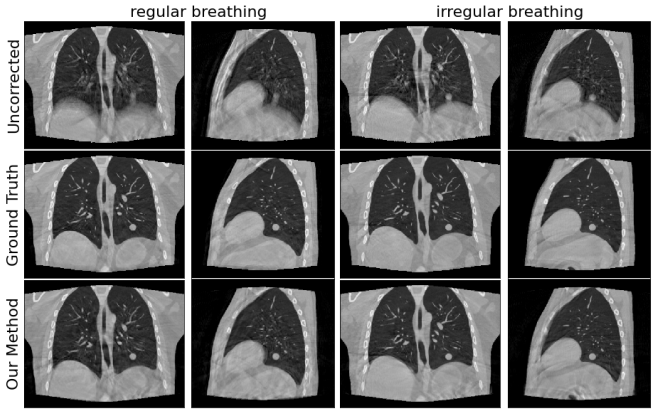

Fig. 2. Comparison of different reconstructions for regular (left) and irregular (right) breathing simulations.

3. RESULTS

3.1. Evaluation on Simulation Data

Table 1 contains the results of the evaluation metrics as described in section 2.2 for the regular and irregular breathing simulations respectively. The results of our method are compared with uncorrected results, i.e., not compensated for respiratory motion.

Table 1. Evaluation metrics for regular and irregular breathing simulation (unit of E_{center} and E_{DVF}: mm).

Simulation	Metric	Uncorrected	Our Method
Regular breathing	DSC	0.46±0.23	0.90±0.05
	E_{center}	8.32±5.68	0.93±0.54
	E_{DVF}	2.38±1.14	1.34±0.63
	NRMSE	0.11	0.07
Irregular breathing	DSC	0.63±0.15	0.92±0.03
	E_{center}	7.72±3.70	0.70±0.31
	E_{DVF}	1.70±0.68	1.07±0.46
	NRMSE	0.10	0.09

The uncorrected results show that there is substantial motion of the tumour and other anatomy during CBCT acquisition. When using our method, the motion of the tumour and other anatomy can be estimated well, and the quality of the reconstructed images are also improved. This is the case for both the regular and irregular breathing simulations.

Figure 2 displays coronal and sagittal views of the uncorrected CBCT reconstructions, i.e., standard FDK without motion compensation (top), the CBCT reconstructions using ground-truth DVFs (middle), and the results of our method (bottom) for the regular breathing and irregular breathing simulations, respectively.

The quantitative evaluation was also consistent with visual assessment. From Figure 2, it can be seen that the image quality of the CBCT obtained by our method is much better

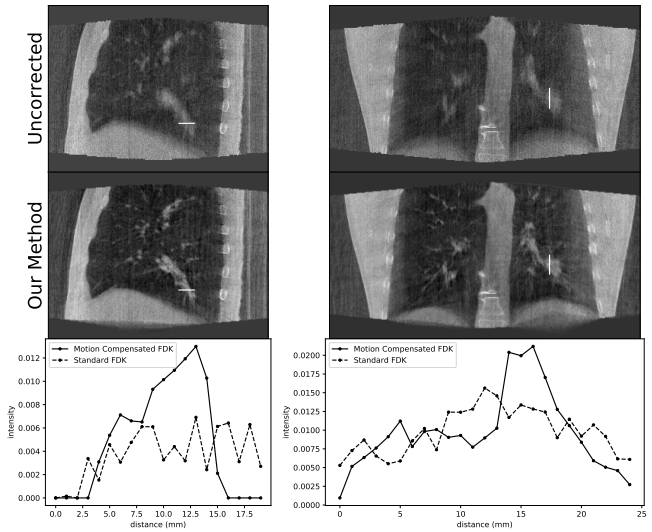

Fig. 3. Uncorrected CBCT (left) and motion compensated reconstruction with our method (right) for patient 1.

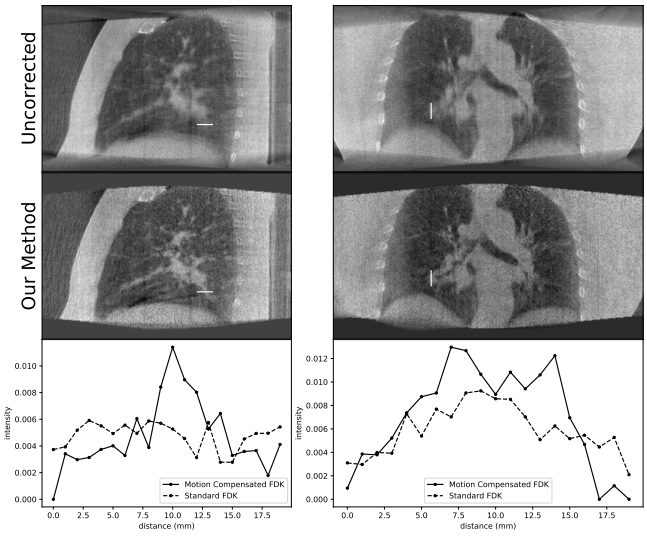

Fig. 4. Uncorrected CBCT (left) and motion compensated reconstruction with our method (right) for patient 2.

than the uncorrected images and comparable to the ground-truth.

3.2. Validation on Clinical Data

Figure 3 and Figure 4 show the sagittal and coronal views of the uncorrected reconstruction (top row) and motion compensated reconstruction (middle row) for the two patients, respectively. Clearer lung tissue details and sharper diaphragm edges can be observed in the reconstructed CBCT after applying our method for both patients. This is highlighted by the intensity profiles at the white lines, which show better tissue contrast after applying our method.

4. CONCLUSION AND DISCUSSION

One of the main limitations of our current method is requiring input surrogate signals and that it can be difficult to acquire good signals either from projections or using external devices. In addition, we currently require non-truncated data and our runtime is still rather long for clinical application. To address the problems above, we are currently working on surrogate-free approach, in which the surrogate signals were optimized along with the motion model and hence did not need to be extracted prior to motion model fitting. Moreover, more advanced reconstruction algorithms, such as iterative reconstruction algorithms, will be utilized to overcome the truncation issue, and GPU implementation will be investigated to accelerate our method.

Our method has great potential for future clinical applications as it can provide both a high-quality motion compensated CBCT image, and accurate estimates of the respiratory motion, including intra- and inter-cycle variations, from nothing other than projection data of a 1-minute CBCT scan. This means it can provide up-to-date estimates of the image and motion of the day on standard linacs, facilitating future innovations in adaptive treatments and outcome studies by providing up-to-date targets and OARs delineation, and more accurate estimates of the delivered dose.

5. ACKNOWLEDGMENTS

This work is supported by the EPSRC-funded UCL Centre for Doctoral Training in Intelligent, Integrated Imaging in Healthcare (i4health) (EP/S021930/1). YH is partially funded by Elekta Ltd. Crawley and the University College London Overseas Research Scholarships. JM is supported by a CRUK Centres Network Accelerator Award Grant (A21993) to the ART-NET consortium. KT is supported by funding from the UK EPSRC (grant EP/T026693/1) to CCP SyneRBI.

6. COMPLIANCE WITH ETHICAL STANDARDS

This research study was conducted retrospectively using human subject data made available in open access by Spare Challenge Dataset (`https://image-x.sydney.edu.au/spare-challenge/`). Ethical approval was not required as confirmed by the license attached with the open access data.

7. REFERENCES

[1] Reinhart A Sweeney, Benedikt Seubert, Silke Stark, Vanessa Homann, Gerd Müller, Michael Flentje, and

Matthias Guckenberger, "Accuracy and inter-observer variability of 3d versus 4d cone-beam ct based image-guidance in sbrt for lung tumors," *Radiation Oncology*, vol. 7, no. 1, pp. 1–8, 2012.

[2] Jan-Jakob Sonke, Lambert Zijp, Peter Remeijer, and Marcel Van Herk, "Respiratory correlated cone beam ct," *Medical physics*, vol. 32, no. 4, pp. 1176–1186, 2005.

[3] Shuai Leng, Joseph Zambelli, Ranjini Tolakanahalli, Brian Nett, Peter Munro, Joshua Star-Lack, Bhudatt Paliwal, and Guang-Hong Chen, "Streaking artifacts reduction in four-dimensional cone-beam computed tomography," *Medical physics*, vol. 35, no. 10, pp. 4649–4659, 2008.

[4] Sheeba Thengumpallil, Kathleen Smith, Pascal Monnin, Jean Bourhis, François Bochud, and Raphaël Moeckli, "Difference in performance between 3d and 4d cbct for lung imaging: a dose and image quality analysis," *Journal of applied clinical medical physics*, vol. 17, no. 6, pp. 97–106, 2016.

[5] Simon Rit, David Sarrut, and Laurent Desbat, "Comparison of analytic and algebraic methods for motion-compensated cone-beam ct reconstruction of the thorax," *IEEE transactions on medical imaging*, vol. 28, no. 10, pp. 1513–1525, 2009.

[6] G Chee, D O'Connell, YM Yang, K Singhrao, DA Low, and JH Lewis, "Mcsart: an iterative model-based, motion-compensated sart algorithm for cbct reconstruction," *Physics in Medicine & Biology*, vol. 64, no. 9, pp. 095013, 2019.

[7] Simon Rit, Jochem WH Wolthaus, Marcel van Herk, and Jan-Jakob Sonke, "On-the-fly motion-compensated cone-beam ct using an a priori model of the respiratory motion," *Medical physics*, vol. 36, no. 6Part1, pp. 2283–2296, 2009.

[8] Jing Wang and Xuejun Gu, "Simultaneous motion estimation and image reconstruction (smeir) for 4d cone-beam ct," *Medical physics*, vol. 40, no. 10, pp. 101912, 2013.

[9] Trine Juhler Nøttrup, Stine Sofia Korreman, Anders Navrsted Pedersen, Lasse Rye Aarup, Håkan Nyström, Mikael Olsen, and Lena Specht, "Intra-and interfraction breathing variations during curative radiotherapy for lung cancer," *Radiotherapy and oncology*, vol. 84, no. 1, pp. 40–48, 2007.

[10] Clément Jailin, Stéphane Roux, David Sarrut, and Simon Rit, "Projection-based dynamic tomography," *Physics in Medicine & Biology*, vol. 66, no. 21, pp. 215018, 2021.

[11] Jamie R McClelland, David J Hawkes, Tobias Schaeffter, and Andrew P King, "Respiratory motion models: a review," *Medical image analysis*, vol. 17, no. 1, pp. 19–42, 2013.

[12] Martina Hurwitz, Christopher L Williams, Pankaj Mishra, Joerg Rottmann, Salam Dhou, Matthew Wagar, Edward G Mannarino, Raymond H Mak, and John H Lewis, "Generation of fluoroscopic 3d images with a respiratory motion model based on an external surrogate signal," *Physics in Medicine & Biology*, vol. 60, no. 2, pp. 521, 2014.

[13] Anthony Kavanagh, Philip M Evans, Vibeke N Hansen, and Steve Webb, "Obtaining breathing patterns from any sequential thoracic x-ray image set," *Physics in Medicine & Biology*, vol. 54, no. 16, pp. 4879, 2009.

[14] Jamie R McClelland, Marc Modat, Simon Arridge, Helen Grimes, Derek D'Souza, David Thomas, Dylan O'Connell, Daniel A Low, Evangelia Kaza, David J Collins, et al., "A generalized framework unifying image registration and respiratory motion models and incorporating image reconstruction, for partial image data or full images," *Physics in Medicine & Biology*, vol. 62, no. 11, pp. 4273, 2017.

[15] Lee A Feldkamp, Lloyd C Davis, and James W Kress, "Practical cone-beam algorithm," *Josa a*, vol. 1, no. 6, pp. 612–619, 1984.

[16] W Paul Segars, G Sturgeon, S Mendonca, Jason Grimes, and Benjamin MW Tsui, "4d xcat phantom for multimodality imaging research," *Medical physics*, vol. 37, no. 9, pp. 4902–4915, 2010.

[17] Björn Eiben, Jenny Bertholet, Martin J Menten, Simeon Nill, Uwe Oelfke, and Jamie R McClelland, "Consistent and invertible deformation vector fields for a breathing anthropomorphic phantom: a post-processing framework for the xcat phantom," *Physics in Medicine & Biology*, vol. 65, no. 16, pp. 165005, 2020.

[18] Simon Rit, M Vila Oliva, Sébastien Brousmiche, Rudi Labarbe, David Sarrut, and Gregory C Sharp, "The reconstruction toolkit (rtk), an open-source cone-beam ct reconstruction toolkit based on the insight toolkit (itk)," in *Journal of Physics: Conference Series*. IOP Publishing, 2014, vol. 489, p. 012079.

[19] Chun-Chien Shieh, Yesenia Gonzalez, Bin Li, Xun Jia, Simon Rit, Cyril Mory, Matthew Riblett, Geoffrey Hugo, Yawei Zhang, Zhuoran Jiang, et al., "Spare: Sparse-view reconstruction challenge for 4d cone-beam ct from a 1-min scan," *Medical physics*, vol. 46, no. 9, pp. 3799–3811, 2019.